STRUCTURAL PETROLOGY AT THE CRYSTAL FALLS MUNICIPAL DAM IRON COUNTY, MICHIGAN

THESIS FOR THE DEGREE OF M. S.
MICHIGAN STATE UNIVERSITY

ROBERT D. WALKER

1956

THESIS

STRUCTURAL PETROLOGY
AT THE CRYSTAL FALLS MUNICIPAL DAM
IRON COUNTY, MICHIGAN

By

Robert D. Walker

A THESIS

Submitted to the School of Graduate Studies of Michigan State University of Agriculture and Applied Science in partial fulfillment of the requirements for the degree of

MASTER OF SCIENCE

Department of Geology

1956

THESIS

ACKNOWLEDGMENTS

The author wishes to express his most sincere thanks to Dr. James Trow for suggesting the problem and for direction and aid in completing this study. Also to Dr. Justin Zinn for his constructive criticisms throughout the investigation.

He also wishes to thank Dr. S. G. Bergquist and the rest of the staff members for their advice and suggestions; J. R. Byerlay for his time in preparing the microphotographs.

STRUCTURAL PETROLOGY
AT THE CRYSTAL FALLS MUNICIPAL DAM
IRON COUNTY, MICHIGAN

Robert D. Walker

ABSTRACT

Seven oriented samples of Huronian iron-formation were collected at the outcrop below the Crystal Falls municipal dam. Thin sections were made two to three times normal thickness, and the orientation of each microfracture in the rock was obtained by use of a four axes universal stage. Poles to the fractures were plotted on a ten centimeter Schmidt net in an effort to correlate the microfractures with known local structures.

Three ages of fractures are recognized. The oldest fractures are associated with the secondary east-west folding, and are thought to be AC tension joints. These have since been rotated by subsequent drag folding. The fractures of intermediate age are divided into two groups which are probably contemporaneous tension joints. One set is found only in the apical portion of the drag fold, and is subparallel to the axial plane. They are classified as AB joints associated with an east-west couple which produced the drag folding. Due to the same couple,

parting occurred along bedding planes. The resulting fractures intersect in the B strain axes. The youngest recognized fractures are related to the northwest trending fault exposed at the outcrop. These fractures lie in a plane which is generally perpendicular to the fault plane, and accordingly are called BC joints with respect to the fault.

TABLE OF CONTENTS

INTRODUCTION

Crystal Falls is located (map 1) in Iron County, which is in the western part of the northern peninsula of Michigan. Geologically, Crystal Falls lies in the northeast apex of a triangular shaped synclinorium of pre-Cambrian metamorphosed sediments.

Glacial material covers much of the bed rock in the Crystal Falls vicinity. Locally the drift may reach a maximum thickness of 300 feet. Characteristic poor drainage is responsible for extensive marshy areas and limited outcrops. The municipal dam is located in a preglacial valley which is now occupied by the Paint River. Although the maximum relief is only 150 feet, the topographic expression is very rugged. Many knobs, basins, and old stream channels reflect conditions before complete withdrawal of the ice.

This thesis is concerned primarily with the orientation of microfractures in the iron-formation, and their relationship to known structures in the Crystal Falls area. Of secondary nature is a study of the orientation of quartz in the microfractures. No attempt is made to determine the mode of deformation; or to interpret the regional geology on the basis of data obtained in this study

The area considered in this report is limited to a single outcrop of Huronian iron-formation which is exposed below the Crystal Falls municipal dam in section 20, T.43N., R.32W. The outcrop is composed entirely of unoxidized iron-formation which has been intensely folded and faulted. The major structure is a series of drag folds which plunge steeply to the northwest. The dip of the bedding ranges from nearly vertical to overturned.

R-32-W

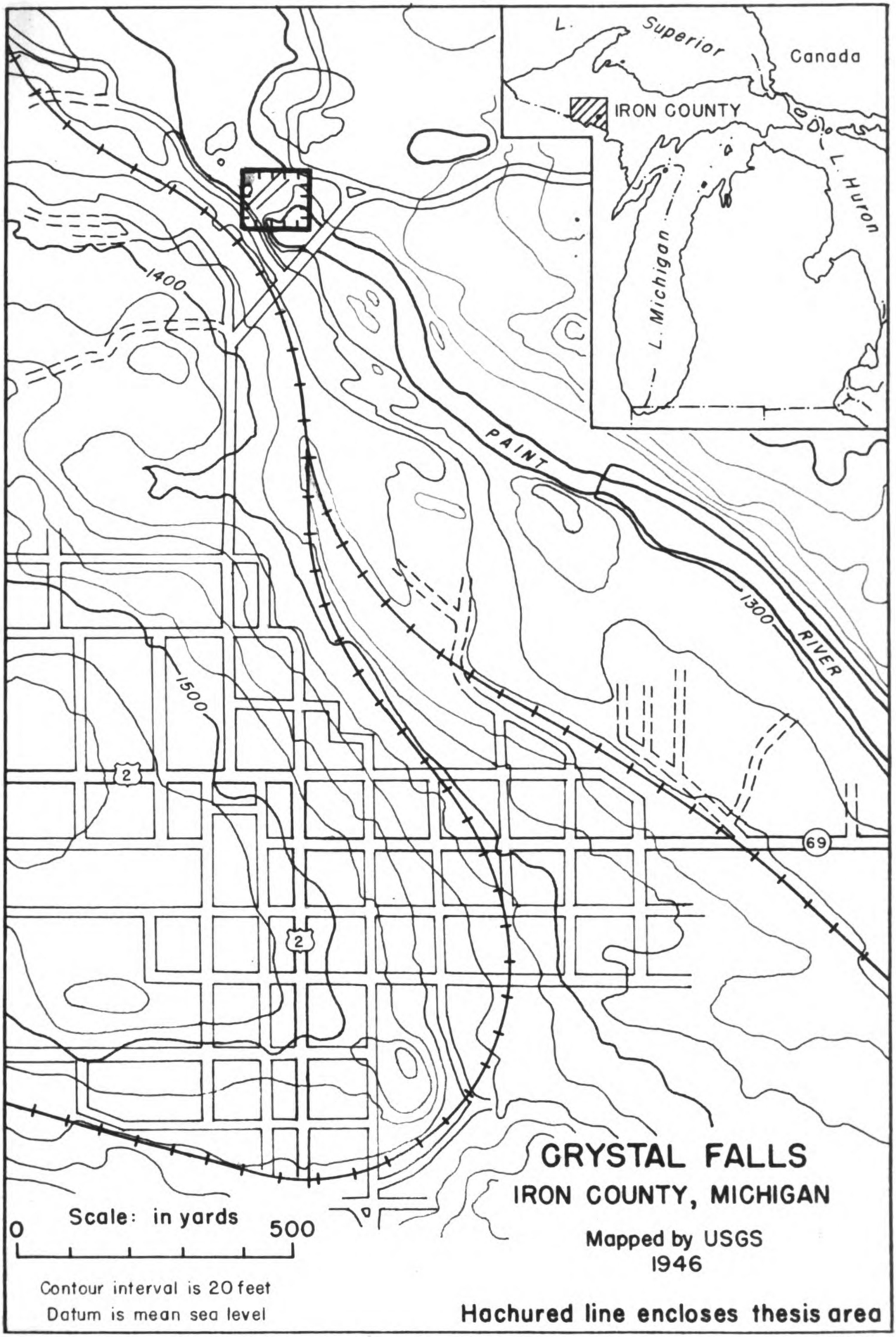

T-43-N

CRYSTAL FALLS
IRON COUNTY, MICHIGAN

Mapped by USGS
1946

Hachured line encloses thesis area

Drawn by Robert Walker

MAP 1

GENERAL GEOLOGY

A great deal of geologic literature concerning the Crystal Falls area is available. Most recent is a series of circulars published by the United States Geological Survey in cooperation with the Michigan Geological Division, Department of Conservation. C. E. Dutton issued a progress report in 1950, of work accomplished in Iron and Dickenson Counties up to that date. The report not only outlines the geology, but also contains an excellent bibliography of previous work in that region. F. J. Pettijohn has written two reports concerning the Crystal Falls area. His 1946 report includes the Alpha district which lies on the southeastern limb of the synclinorium about twelve miles south of Crystal Falls. The second report, published in 1952, deals with the area just north of the city, and contains a map of the outcrop area (map 2) which was compiled by H. L. James and W. S. White on a scale of one inch to ten feet.

Stratigraphy

Pettijohn has recognized four mappable rock units in the Crystal Falls area. They are (1) a greenstone complex, (2) the footwall strata, (3) an iron-formation, and (4) the hanging-wall strata. The last three formations are believed to be Huronian sediments, but the exact age of the iron-

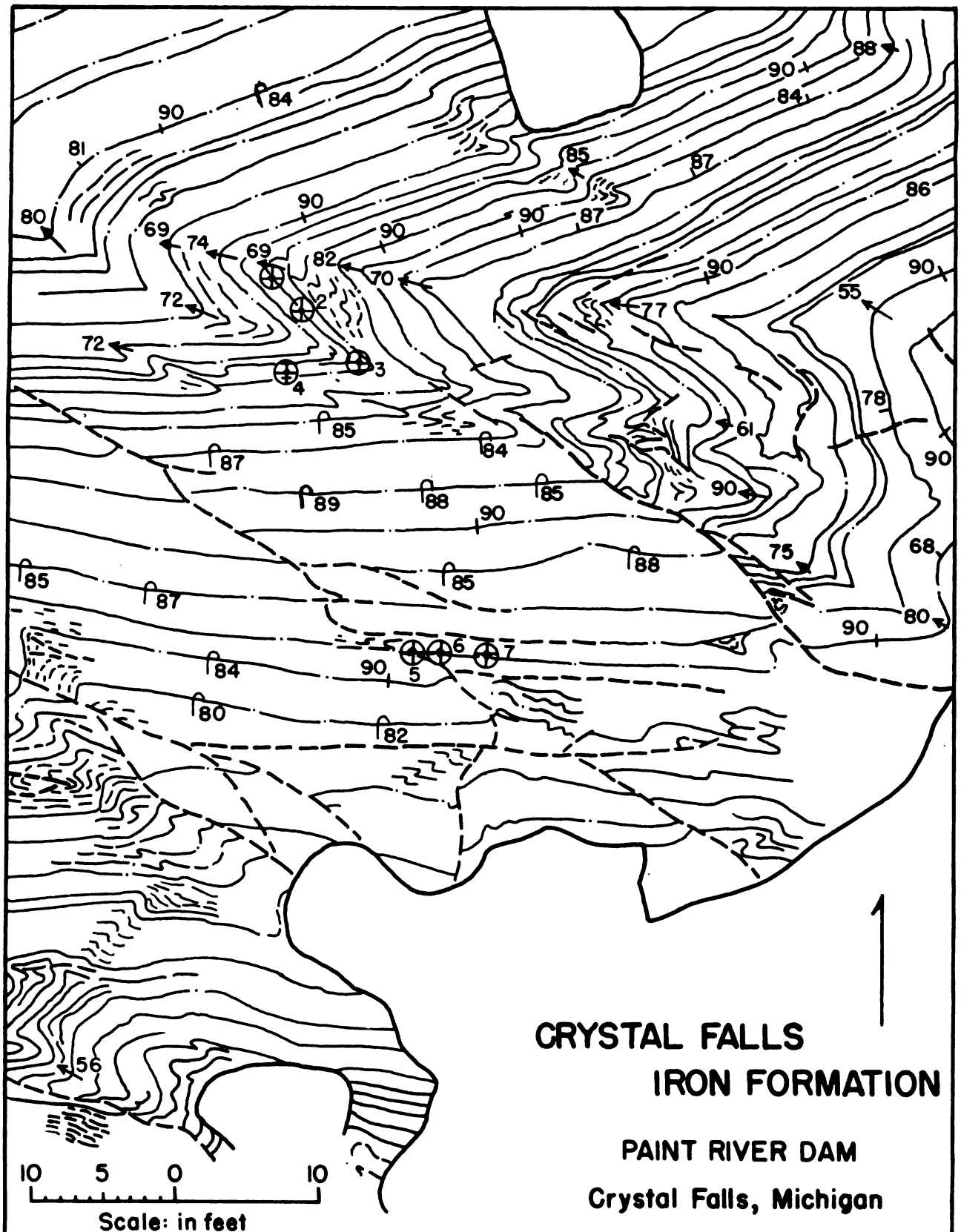

CRYSTAL FALLS IRON FORMATION

PAINT RIVER DAM

Crystal Falls, Michigan

Mapped by U.S.G.S

H.L. James
W.S. White

Sept 1946

Drawn by Robert Walker

MAP 2

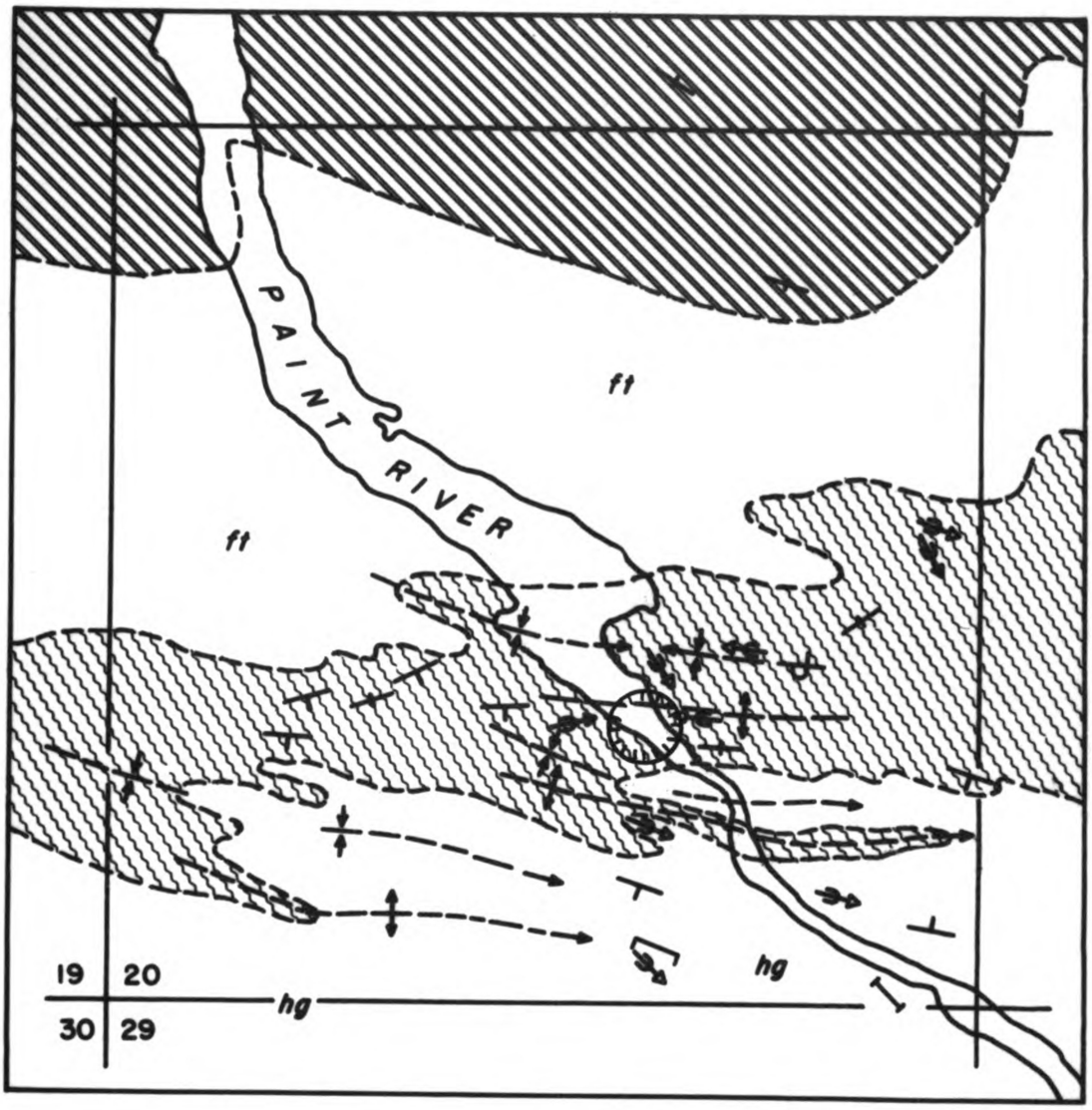

STRUCTURE OF SECT. 20, T. 43N., R. 32W.

IRON COUNTY, MICHIGAN

0 Scale: 1000
in feet

N

hg HANGING - WALL STRATA
IRON - FORMATION
ft FOOTWALL STRATA
GREENSTONE

Map by:
F. J. Pettijohn
1952

Drawn by Robert Walker

MAP 3

formation is in doubt. J. Zinn (1932) correlates the iron-formation of the Crystal Falls district, mainly on the basis of similar lithology and stratigraphic sequence, with the upper Huronian Bijiki iron-formation of the Marquette district. However, Pettijohn (1946) believes:

> If the unconformity at the base of the hanging wall beds be that which is almost universally present just above the productive iron-formation in the other districts of the Lake Superior region, then the iron bearing beds of the Crystal Falls area would be middle Huronian as they are elsewhere and the overlying strata would be upper Huronian. Accordingly the iron-formation would be equivalent of the Negaunee iron-formation of the Marquette district.

Because of the controversial nature of the problem, the name "Crystal Falls Iron-formation" as used in this paper does not imply an age, but merely designates a location. The stratigraphic sequence proposed by Pettijohn (1952) has been incorporated (Table I) into this report.

Structure

In the Crystal Falls area, the major structure is a large faulted syncline which widens and plunges to the southwest. The southern limb forms an arc that can be traced beyond the Alpha district which lies about thirteen miles south of Crystal Falls. The north limb is continuous to Iron River.

The south limb of the syncline has been subjected to a greater degree of deformation. Secondary folds on this limb maintain a northwestward trend, and plunge generally

TABLE I

STRATIGRAPHIC COLUMN OF THE CRYSTAL FALLS DISTRICT

Rock unit	Character of unit	Thickness in feet
Hanging-wall strata	Graywacke, basal and (or) chert breccia overlain by gray and black slates and graywackes. Lower slate magnetic west of the Paint River.	500
Unconformity		
Iron-formation	Chert and siderite, interbedded; locally oxidized to banded chert and hematite; locally rich in iron silicates.	300-600
Footwall strata	Slates, gray and black, with fissile pyritic slate in upper part.	800-900
Unconformity (?)		
Greenstone	A complex of fine-grained, massive, greenish-gray altered lavas, in part ellipsoidal, with a little agglomerate and tuff.	very great

in that direction. Transverse faulting has occurred sub-parallel to the secondary folding. The beds have been tightly folded producing a very irregular outcrop pattern. This characteristic, typical in the iron-formation, is also responsible for the apparent difference in thickness of the formation.

The outcrop below the municipal dam is located (map 3) on the north limb of the syncline in a belt of generally west-northwest trending secondary folds which plunge

gently southeastward. The axial planes of the drag folds exposed at the outcrop are essentially parallel to the axial planes of the secondary folds. A complete description of this relationship is given below.

Petrology

The outcrop below the dam is unoxidized iron-formation consisting entirely of alternating beds of gray siderite and black chert. Generally, the beds average from one to two inches in thickness. Cleavage is not present in the iron-formation, but thinly laminated beds of siderite produce a pseudo-cleavage which has been mistaken for true cleavage. The massive siderite beds take on a blocky appearence due to closely spaced joints.

The iron-formation is not highly metamorphosed. On the contrary, Williams (1954) suggests that the presence of stilpnomelane places the rock in the greenschist facies. In describing rocks in this class, he states:

> Stilpnomelane is widly distributed and occurs especially as sheaves of tabular crystals that have grown in the schistosity surfaces after deformation ceased.

Orientation of the stilpnomelane is not prominent, and can be observed only in a few of the thin sections. The poor orientation is probably due to the cherty nature of the rock which would not allow development of well defined shear features.

The essential minerals are chert, siderite, and a green hydrous iron silicate similar to stilpnomelane or minnesotaite. Probably both of the latter minerals are present. Mineralization has taken place along bedding and fractures in the rock. Common secondary minerals are quartz, siderite, hematite, and pyrite. Table II gives the chemical analysis of the unoxidized iron-formation. The analysis was made from samples collected at the outcrop below the dam.

TABLE II

ANALYSIS OF THE UNOXIDIZED IRON-FORMATION AT CRYSTAL FALLS
(Pettijohn 1952)

SiO_2	31.84	H_2O	1.80**
Al_2O_3	2.09	TiO_2	0.12
Fe_2O_3	14.83	CO_2	19.40
FeO	20.59*	P_2O_5	0.83
MgO	3.08	SO_3	none
CaO	1.49	S	0.33
Na_2O	- - -	MnO	2.53
K_2O	- - -	Total	99.47

* Calculated from remaining CO_2 equivalent. A direct determination is not possible. Any MnO_2 is disregarded.

** Includes organic material.

Chert. Chert is the main constituent of the iron-formation. It is black, commonly very dense, and has a

a pronounced conchoidal fracture. Under the microscope, the chert appears (Plate I) as a fine grained mosaic. In samples #3 and #5, the chert (Plate IV) has a mylonitic character.

Siderite. Siderite occurs in thin beds, granular masses, and individual rhombohedrons (Plate VI) disseminated in the cherty matrix of the rock. In the hand specimen it has a steel gray color. It is easily recognized under the microscope by the high birefringence.

Stilpnomelane. Stilpnomelane most commonly occurs in the needle-like form (Plate VII). The tabular form, however, is not rare in the thin section. The mineral cannot be recognized in the hand specimen.

The mineral species was recognized over 100 years ago, and was variously placed in the mica and chlorite groups. The chemical characteristics are similar to chlorite, but optically it is often confused with biotite. It can be distingushed from biotite however, by the transverse fractures cutting across the perfect (001) cleavage. It also has a higher birefringence.

The chemical composition (Table III) of the mineral is uncertain. There is a wide range in the ratios of Fe'' to Fe'''. Oxidation of the iron is variable. Winchell (1951) is an excellent source for information concerning the chemical nature of this mineral.

The indices of refraction have a wide range, and are directly related (Table III) to the ratios of Fe'' to Fe''' to Mg; ferristilpnomelane having the higher indices. The mineral has a definite pleochroism when oriented. However, in disseminated needles, the pleochroism is less prominent and may not be visible.

TABLE III

PROPERTIES OF STILPNOMELANE

(Winchell 1951)

Sample	#1	#2	#3
(Fe, Mn)O	34.43	25.13	3.86
Fe_2O_3	0.35	13.33	31.67
(-) 2V	0°	0°	0°
Alpha	1.546	1.565	1.625
Gamma	1.576	1.623	1.735
Color	green	yellow	brn-blk
Pleochroism			
alpha	pale green	colorless to clear yellow	bright gold yellow
gamma	deep green	light greenish yellow	deep olive brown

Minnesotaite. Minnesotaite occurs (Plate VII) in a manner similar to that of stilpnomelane in the thin section. A positive identification of this mineral was not possible. Gruner (1946) states:

> If there is no orientation and, therefore no pleochroism it becomes impossible to tell this mineral (stilpnomelane) from granules of minnesotaite or even greenalite unless X-rays can be used for analysis.

Chemically, minnesotaite is an iron variety of talc. Winchell suggests the following formula:

$$Fe_3(OH)_2SiO_4O_{10}$$

Gruner modifies this formula to:

$$(OH)_{22}(Fe'',Mg)_{22.3}[Si_{30.4}(Al, Fe''')_{1.4}]O_{74}$$

Gruner's analysis of minnesotaite appears in Table IV.

Here again, the optical properties depend on the ratios of Fe'' to Fe''' to Mg. Gruner describes a colorless variety with a small optic angle and a high birefringence which is similar to muscovite. Alpha is normal to the perfect (001) cleavage. Elongation is positive. The optic angle is very small. Pleochroism is generally absent, however, the mineral may be slightly so. Then alpha is very pale yellow, and gamma is pale green. A comparison is made between the properties of minnesotaite and stilpnomelane in Table IV.

Gruner accounts for the complex structures of the hydrous iron silicates in this manner:

> As stilpnomelane forms from, let us assume a colloidal gel, it will take the ions in its neighborhood which are most convenient and of the necessary charge. If it cannot find any more it will stop growing. The leftover gel material, then, may be of the proper composition to form minnesotaite or greenalite or quartz and siderite, if CO_2 is available in considerable concentration. This illustration should suffice to show why these silicates can show so many variables in otherwise definite crystal structures. It also sheds light on the bewildering arrangements the minerals, particularly the silicates, may take with respect to shapes, grain sizes, textures, and even bedding and banding without very material changes in the chemical composition of the taconite as a whole.

TABLE IV

COMPOSITION AND SOME PROPERTIES OF MINNESOTAITE AND STILPNOMELANE

(Gruner 1946)

	Minnesotaite			Stilpnomelane	
	#1	#2	#3	#4	#5
SiO_2	51.29	54.6	46.85	44.77	45.24
Al_2O_3	0.61	....	4.64	6.32	6.73
Fe_2O_3	2.00	0.5	11.60	20.79	25.34
FeO	33.66	35.5	20.00	12.83	3.45
MgO	6.26	3.4	5.75	5.01	7.67
MnO	0.12	....	0.33	0.21	0.60
CaO	none	....	0.94	0.10	1.91
Na_2O	0.08	....	0.27	0.07	0.03
K_2O	0.03	....	2.07	3.31	1.67
TiO_2	0.04	....	0.15	0.04	0.33
H_2O+	5.54	....	5.77	5.64	6.72
H_2O-	0.24	....	1.80	1.96	0.76
	99.87		100.17	100.05	100.45
Alpha	1.580	....	1.564	1.58	1.599
Gamma	1.615	....	1.615	1.677	1.680
Biref.	0.035	....	.....	0.097	0.081
2V	.....	....	very small	very small	0°
Pleochroism:					
Alpha	.....	....	.....	yellow	gold-yel
Gamma	.....	....	.....	olive-brn	red-brn

Quartz. Quartz occurs as a secondary fracture filling mineral. It has generally two modes of occurrence. While most of the quartz was medium sized anhedral grains; in a few cases very large euhedral quartz was observed (Plate VI) growing normal to the fracture wall. This fact may indicate more than one period of mineralization.

Pyrite. Pyrite (Plate III) is found in association with the secondary quartz. The anhedral crystals have been partially altered to hematite in some cases.

Hematite. Primary hematite (Plate VII) is found in small quantities along bedding planes. Secondary hematite occurs in fractures and as disseminated particles (Plate III) in the cherty matrix of the rock. The source of the secondary hematite is uncertain; it may be closely associated with the ore-forming process.

Limonite. Limonite (Plate VI) covers most of the exposed rock. Quite commonly it forms a very hard rusty colored veneer on the rock surface. It is the oxidation product of normally weathered siderite.

METHOD OF ANALYSIS

Field Techinque

Seven oriented samples were collected at the outcrop below the dam. The procedure for orienting the samples is described by Fairbairn (1954) and Billings (1954). In this case, since the iron-formation is nonmagnetic, a Brunton compass was used in marking the samples. All of the samples were oriented with respect to magnetic north, since the magnetic declination at Crystal Falls is only one degree east of north.

The first step was selection of the samples. This was done with respect to the folding and faulting. Four samples were collected on the fold limbs, and three at varying distances from the fault. The second step was to etch the attitude of the rock on the specimen (fig 1) with a steel nail. Then the specimen was cleaved from the formation and re-marked. Adhesive tape makes a good label if the rock is dry and relativity clean. Finally, the location and attitude of the rock, and the position of the label was noted in a field notebook. The label was usually placed on the top of the specimen, but in the case of overturned beds, the label was placed on the bottom of the sample.

Laboratory Technique

Three thin sections were made from each sample. The chips were cut (fig 1) with respect to strike and dip in the following manner:

Chip A - Parallel to strike and perpendicular to bedding.

Chip B - Perpendicular to strike and bedding in the plane of dip.

Chip C - Parallel to the bedding plane.

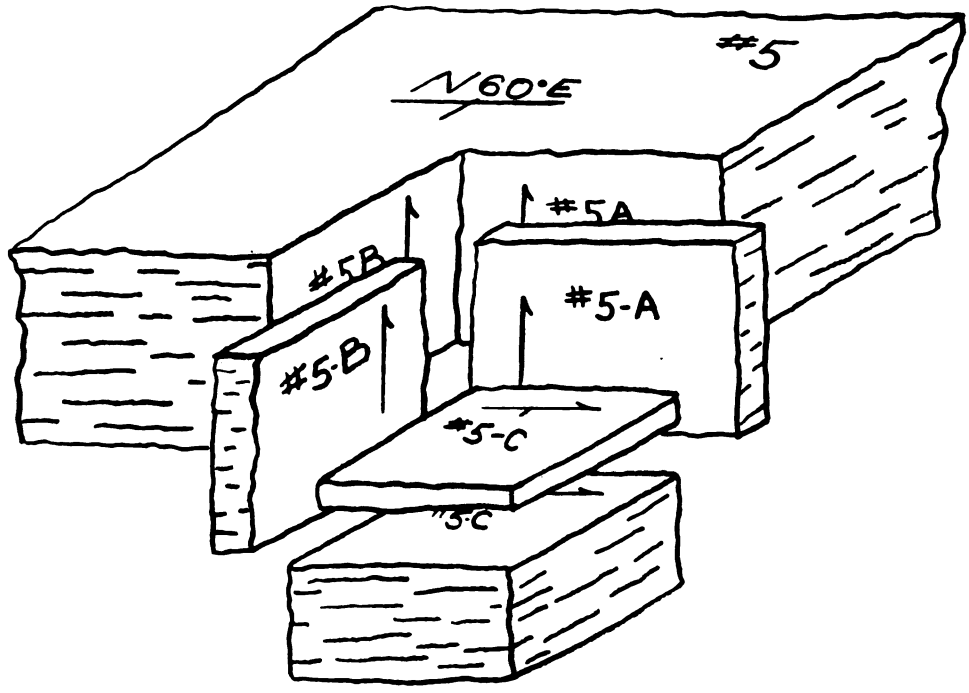

Fig. 1 System of labeling specimen and rock chips.

The chips were marked according to the system described by Tuttle (1950), and sent to a commerical laboratory for grinding. In the first phase of grinding, the sections were made doubly thick (60-90 microns) as suggested by Tuttle (1955), to insure an accurate orientation of the

microfractures. After determining the orientation of the fractures, the thin sections were reground to normal thickness, and a study was made of the quartz orientation in the fractures.

Orientation of the microfractures was carried out in the following manner, using a four axes universal stage.

Orientation.

1. Rotate on the inner vertical axis until the fracture is parallel to the north-south cross hair.

2. Rotate on the north-south axis until the fracture is:

   a. a narrow line if the fracture is very narrow.

   b. at the widest dimension if the fracture has a noticeable width.

Plotting of Data.

1. Read the inner vertical scale. Rotate the overlay until the 0^{o} reading is over the number of degrees read on the inner vertical scale.

2. Read the north-south scale. If the universal stage dips:

   a. east, plot the corresponding number of degrees in from the west periphery.

   b. west, plot the corresponding number of degrees in from the east periphery.

The most accurate results are obtained when a low power objective is used without the analyzer. In the case of very thin fractures, a higher power objective may be employed.

The procedure for determining quartz orientation is outlined by Fairbairn (1954). It is especially helpful to

draw a small sketch of the orientation of the thin section on the overlay. This will eliminate many errors in rotation of the diagram.

All of the diagrams were rotated to a horizontal plane and marked with respect to magnetic north. This was done for two reasons; first, to facilitate comparison between individual diagrams, and secondly, to aid in the statistical analysis.

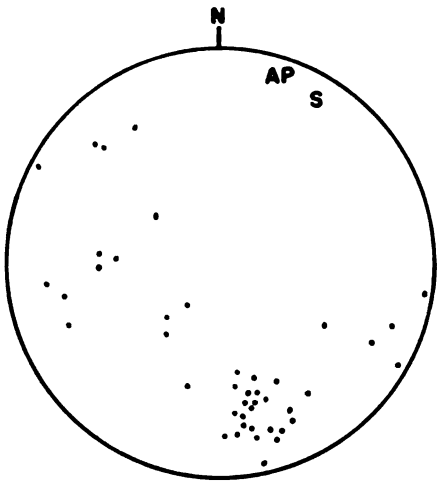

Fig. 2

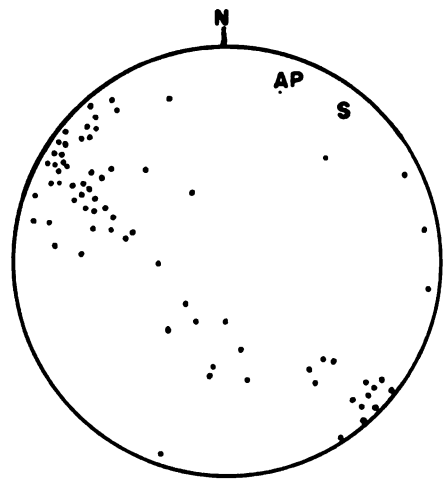

Fig. 3

Fig. 2 - 45 poles to microfractures in sample #1.
AP = pole to axial plane, S = pole to bedding.

Fig. 3 - 72 poles to microfractures in sample #2.

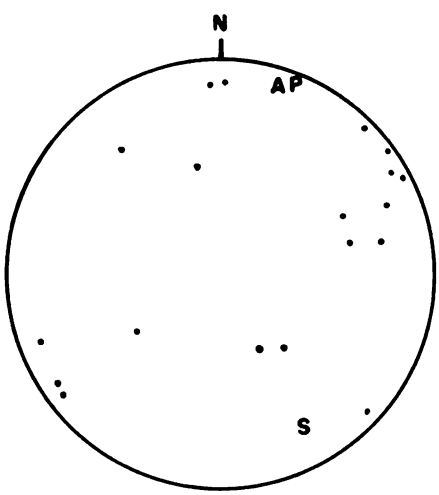

Fig. 4

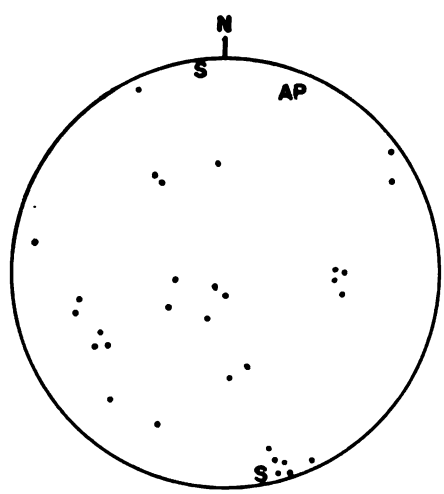

Fig. 5

Fig. 4 - 19 poles to microfractures in sample #3.

Fig. 5 - 31 poles to microfractures in sample #4.

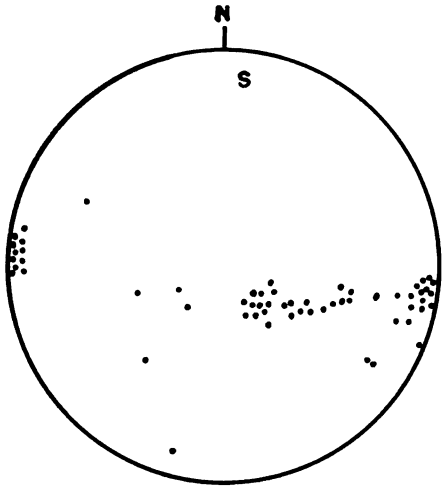

Fig. 6

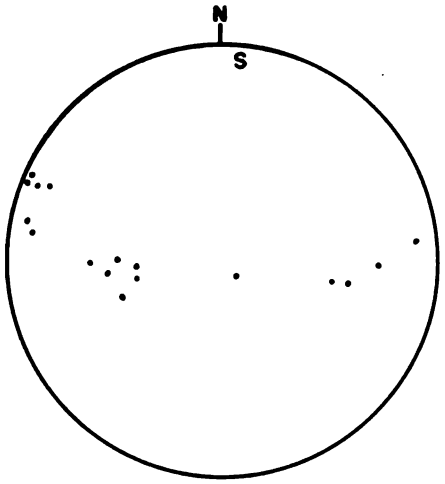

Fig. 7

Fig. 6 - 72 poles to microfractures in sample #5.

Fig. 7 - 18 poles to microfractures in sample #6.

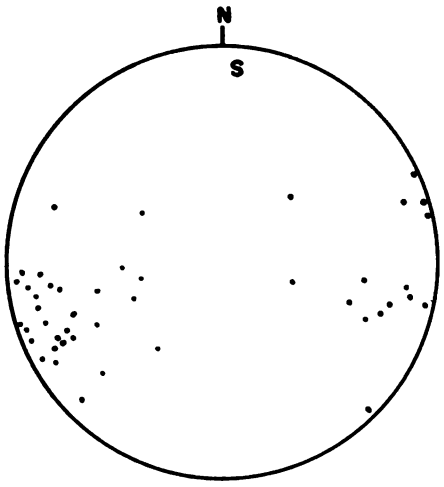

Fig. 8

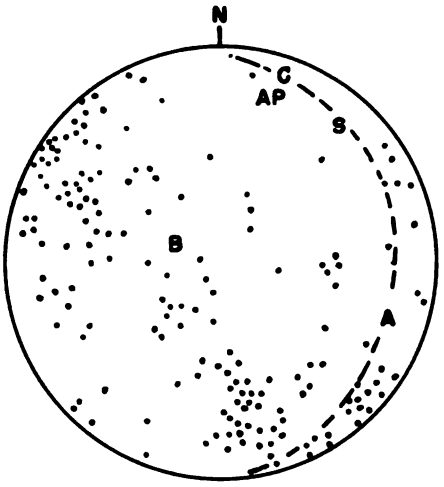

Fig. 9

Fig. 8 - 43 poles to microfractures in sample #7.

Fig. 9 - Composite diagram of 167 poles to microfractures from samples #1, #2, #3, and #4.

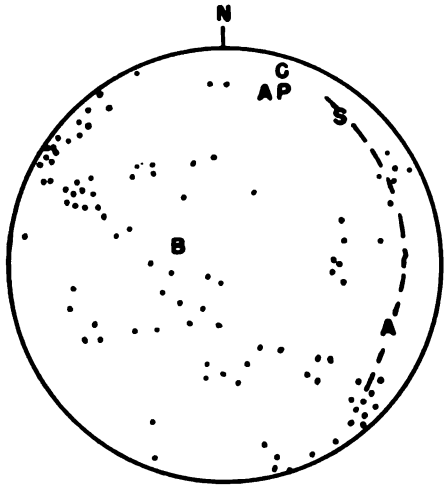

Fig. 10

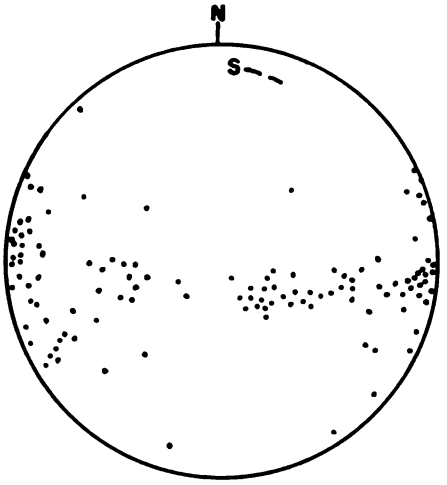

Fig. 11

Fig. 10 Composite diagram of 122 poles to microfractures from samples #2, #3, and #4. A, B, and C are in relation to the fold.

Fig. 11 Composite diagram of 133 poles to microfractures from samples #5, #6, and #7.

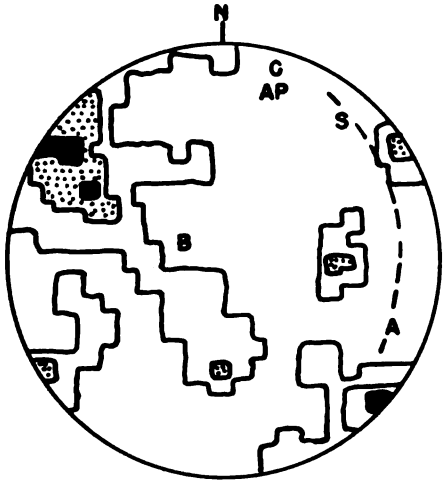

Fig. 12

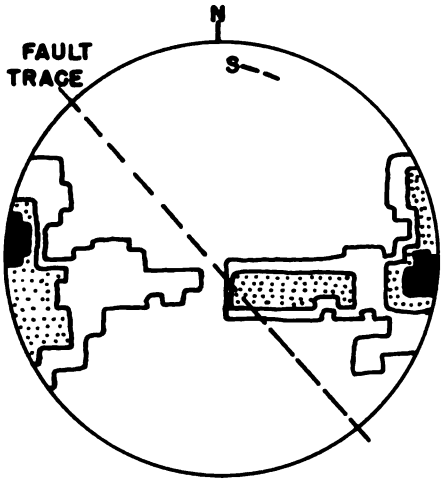

Fig. 13

Fig. 12 Figure 10 contoured. Contours: 0-5-8-12-15%.

Fig. 13 Figure 11 contoured. Contours: 0-2-5-7-10%.

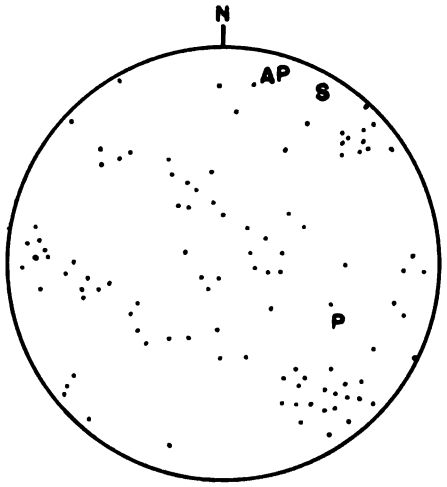

Fig. 14

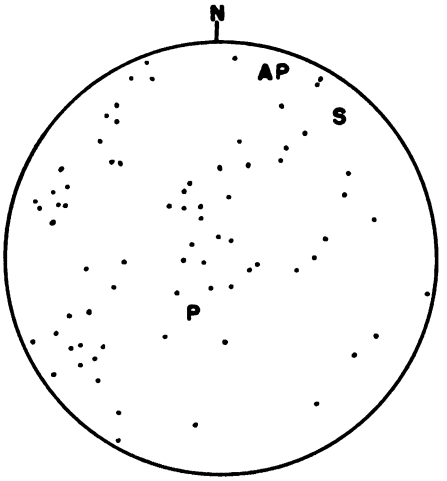

Fig. 15

Fig. 14 - 107 quartz axes in a fracture from sample #1.
P = pole to fracture.

Fig. 15 - 78 quartz axes in a fracture from sample #2.

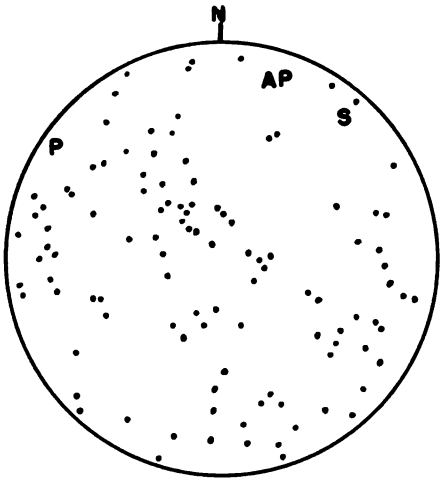

Fig. 16

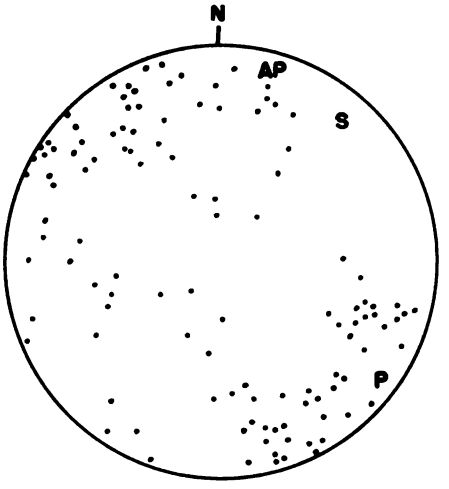

Fig. 17

Fig. 16 - 107 quartz axes in a fracture from sample #2.

Fig. 17 - 130 quartz axes in a fracture from sample #2.

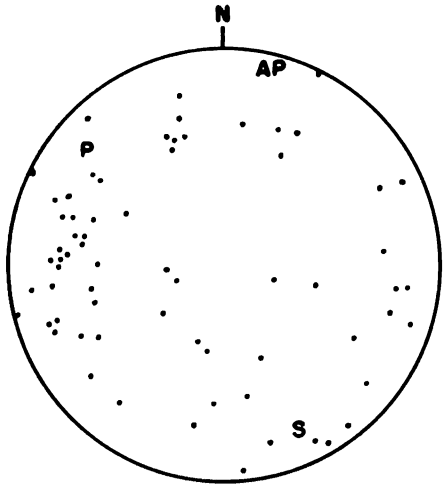

Fig. 18

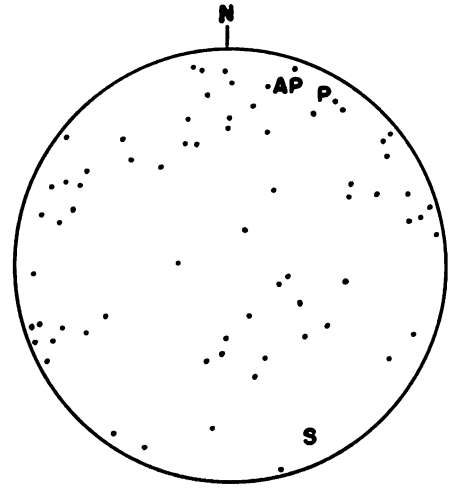

Fig. 19

Fig. 18 - 67 quartz axes in a fracture from sample #3.

Fig. 19 - 71 quartz axes in a fracture from sample #3.

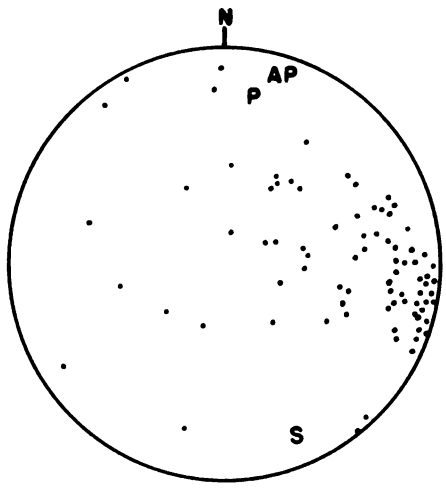

Fig. 20

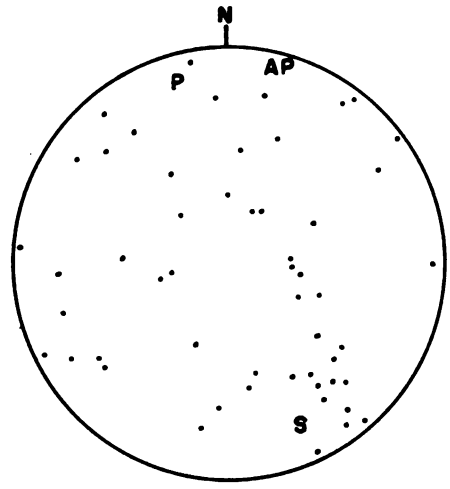

Fig. 21

Fig. 20 - 82 quartz axes in a fracture from sample #3.

Fig. 21 - 55 quartz axes in a fracture from sample #3.

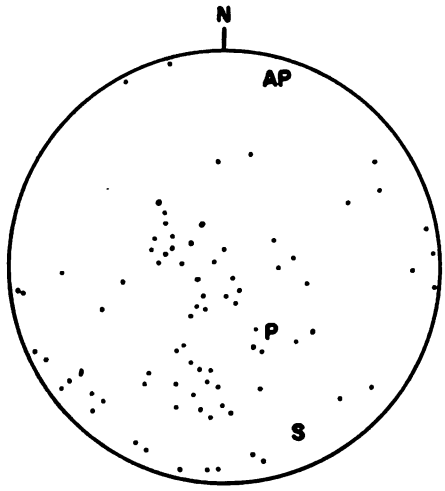

Fig. 22

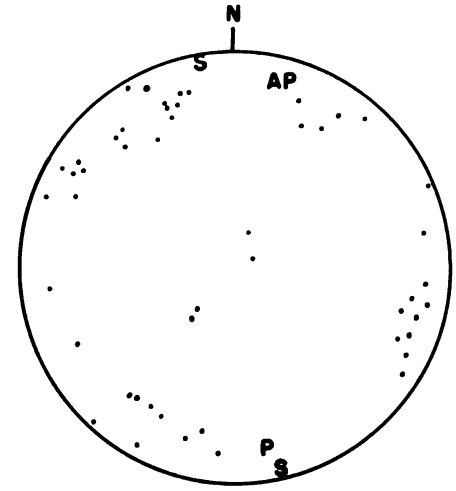

Fig. 23

Fig. 22 - 83 quartz axes in a fracture from sample #3.

Fig. 23 - 57 quartz axes in a fracture from sample #4.

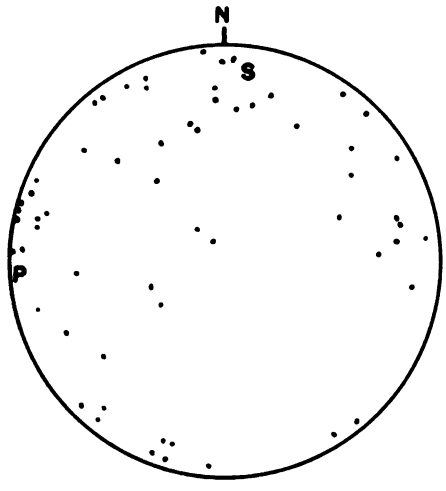

Fig. 24

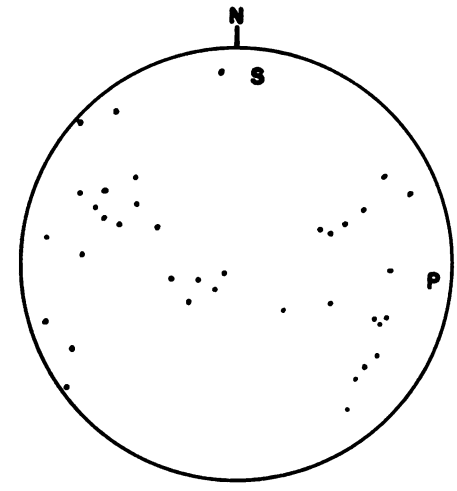

Fig. 25

Fig. 24 - 64 quartz axes in a fracture from sample #5.

Fig. 25 - 40 quartz axes in a fracture from sample #5.

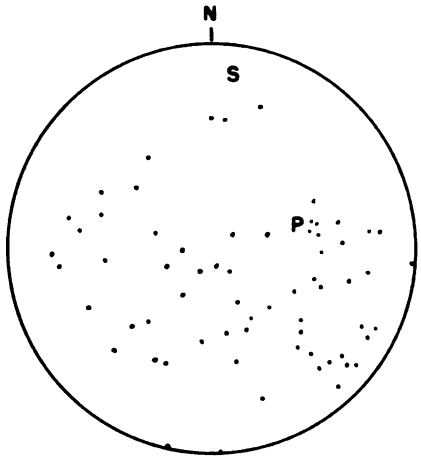

Fig. 26

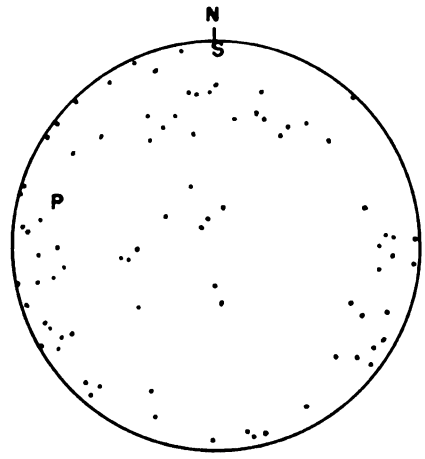

Fig. 27

Fig. 26 - 65 quartz axes in a fracture from sample #5.

Fig. 27 - 85 quartz axes in a fracture from sample #7.

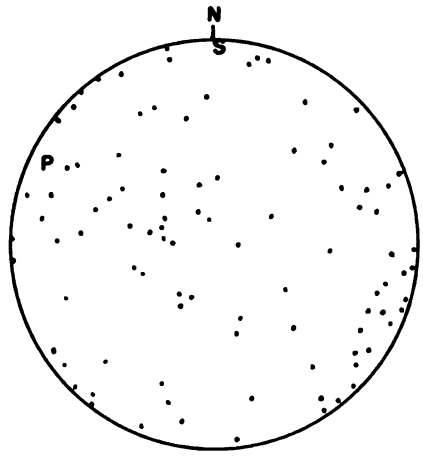

Fig. 28

Fig. 28 - 98 quartz axes in a fracture from sample #7.

ANALYSIS OF DATA

Local Structure

The outcrop below the dam is on the north limb (map 3) of a large syncline which plunges to the southwest. Secondary folds on the north limb trend generally west-northwest, and plunge gently southeastward. Locally, however, the plunge may be reversed. The minor flexure exposed below the dam plunges northwestward. According to Billings (1954), the fact that the axial plane of the minor fold is subparallel to the axial planes of the secondary folds would indicate a relationship which is in harmony. This same fact also points out an obvious disharmony with regional structure which can only be accounted for by more than one period of deformation.

Pettijohn (1952) has noted that the slaty cleavage in the hanging-wall slates is generally parallel to the axial planes of the secondary folds. The presence of drag folding and cleavage related to the secondary folding is evidence that the deformation which was responsible for the regional structure was not strong enough to produce secondary lineations; or the force which caused the secondary folding was strong enough to destroy lineations related to the first tectonic period.

Structure at the Outcrop

Two general types of fractures were observed in the iron-formation which is exposed below the municipal dam. One type is very thin, almost tight, and contains secondary hematite and a green iron silicate. The second type is generally much wider and contains quartz, siderite, and small quantities of hematite and pyrite. The quartz mineralized fractures apparently cut all of the fractures containing other secondary minerals. It is not believed however, that this relationship is a valid criterion for determining relative ages of the fractures, because there is essentially no difference in orientation.

Three different ages of fractures are recognized. The oldest, and most prominent, have been rotated by younger drag folding to produce an apparent trend to the northeast on the fold. Contemporaneous fractures in the area adjacent to the fault have not been affected by this rotation. These fractures have a north-south vertical attitude. The intermediate aged fractures are steeply dipping, and have a trend subparallel to the axial plane of the drag fold. the youngest fractures are shallow dipping, and tend to lie in a plane which is perpendicular to the northwest trending fault. This set of fractures strike generally northeastward, and dip to the northwest.

The orientation of the fractures in sample #1 (fig 2) are disregarded throughout most of this study. The pattern

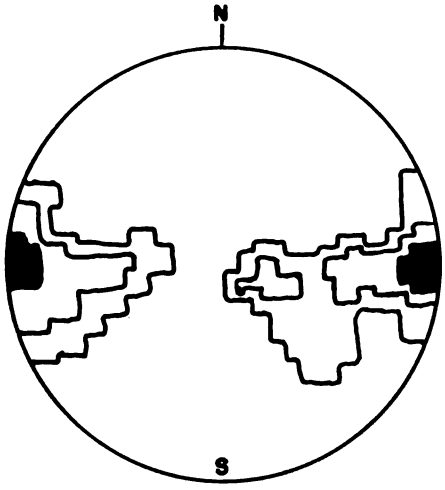

Fig. 29

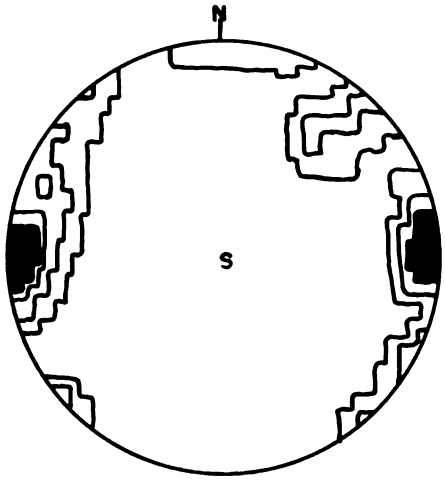

Fig. 30

Fig. 29 Orientation of fractures when bedding is rotated to an east-west, vertical position. Contours: 0-2-3-6%.

Fig. 30 Orientation of fractures when bedding is rotated to the horizontal. Contours: 0-2-3-6%.

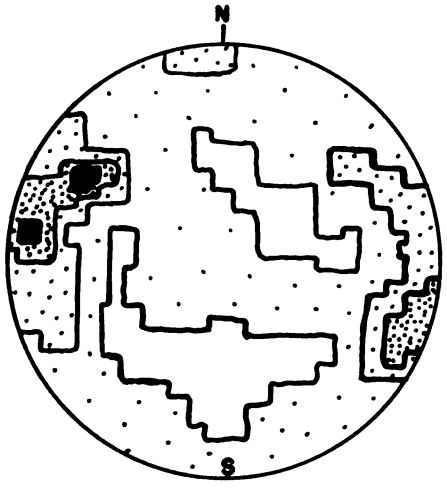

Fig. 31

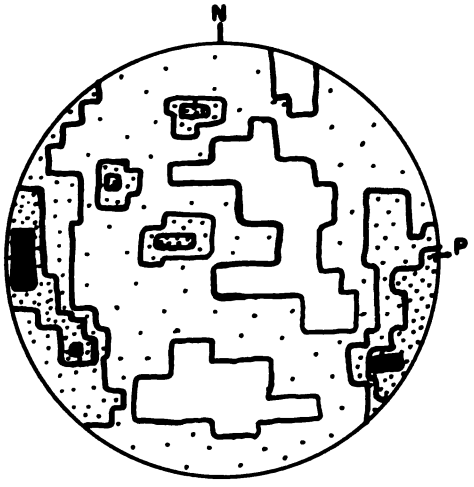

Fig. 32

Fig. 31 Orientation of quartz axes in fractures. Beds have been rotated to an east-west vertical position. Contours: 0-½-1½-2-3%.

Fig. 32 Orientation of quartz in fractures. Fractures have been rotated to a north-south vertical position. Contours: 0-½-1½-2-3%.

of the fractures in this section of the fold do not reflect (fig. 9) values found in other samples. This may be due to the close proximity (Map 2) of an imperfectly formed drag fold.

First period of fracturing. The oldest recognized fractures are not related to the structural features exposed at the outcrop below the dam. The original orientation of

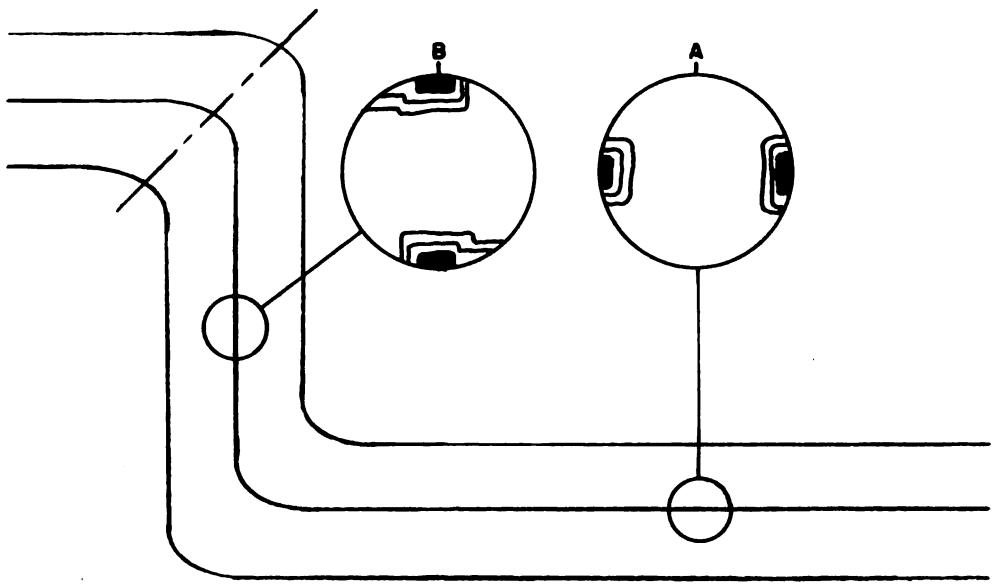

Fig. 33 Diagrammatic cross section of a drag fold showing hypothetical fabric diagrams in (A) an unfolded area, and (B) the resultant fabric due to drag folding.

these fractures however, has been partially obscured by subsequent drag folding. The resultant orientation is shown in figures 2 - 5. A comparison between the composite diagrams, figures 10-13, of the fractures on the fold and in the area adjacent to the northwest trending fault has revealed a possible rotation of the fractures (fig.33) due to later drag folding. In support of this theory, many

of the fractures have been displaced by slippage along the bedding planes which probably occurred at the time of drag folding. The fractures observed in the samples taken at varying distances from the fault were not affected by the drag folding, and are believed to maintain essentially the orginal attitude of this set of fractures. However, fractures in this area have been somewhat affected by slippage along bedding planes.

The two peripheral maxima in figures 12 and 13 have a difference in orientation of only thirty degrees. A comparison of the two diagrams, after rotation of the bedding to an east-west vertical attitude (fig. 29), reveals a pronounced north-south vertical orientation of these fractures. The same orientation is obtained when the bedding is rotated (fig.30) to a horizontal position. A statistical analysis supports the assumption that these fractures are directly related to each other.

The secondary quartz axes in these fractures (fig. 31 and fig. 32) are oriented essentially perpendicular to the fracture walls. The maxima produced in figure 31 were obtained only after all of the samples were rotated to an east-west vertical position. A random orientation persisted when the comparison was made without rotating the samples. Figure 32 is the result of rotating the fractures in this class, to a north-south vertical attitude. Both cases point out the perpendicular relationship between the quartz

axes and the fracture wall. The smeared maxima may be the result of rotation during the period of drag folding. The orientation of the optic axes of secondary quartz in individual fractures is shown in figures 14, 16, 17, 18, 24, 25, 27, and 28.

The fractures in this group are then assumed to have had a north-south vertical attitude before drag folding. The orgin of these fractures could be associated with the development of a large east-west fault which lies approximately 3000 feet south of the problem area. If this is the case, these fractures would be classified as BC joints as described by Balk (1952). However, this orgin appears to be unlikely because of the great distance separating the fault and the outcrop below the dam. More likely, these fractures are contemporaneous with the nearly horizontal east-west secondary folding. In this case, the fractures would be classified as AC tension joints resulting from a north-south compression accompanied by an east-west stretching along the fold axis.

Second period of fracturing. The fractures of intermediate age are found only in the apical portion of the drag fold, or parallel to bedding on the limbs of the fold. There is a general tendency for the fractures in the apex of the fold to align parallel to the axial plane. In this thesis, these fractures are termed AB tension joints. The fabric pattern is not strong enough to be distinguished on the

composite diagrams. It can be seen however, on the individual sample (fig. 4) diagram.

Associated with the drag folding is a parting along the planes of bedding. The intersection of these fractures produces a lineation in B, or parallel to the fold axis.

Orientation of quartz within the fractures of intermediate age (fig. 19, 20, 21, and 23) is not well defined and may vary considerably according to the type of fracture. For example, figure 19 illustrates the orientation in an en-echelon fracture. Figure 20 is the fabric of secondary quartz in a continuous fracture in the fold apex. Figure 23 shows the orientation of quartz in a fracture which resulted from splitting along a bedding plane.

The absence of AC tension joints in the apical area of the fold may be due to mylonitization of the rock which could have obscured any pre-existing fractures. The fractures of intermediate age are the only fractures which may be attributed directly to the drag folding.

Third period of fracturing. The youngest set of fractures appears to cut all features (Plates I, III, and V) within the iron-formation. Displacement is evident along most of the fractures in this class, but the amount of movement is generally very slight. The fractures trend northeastward, and dip gently to the northwest. These fractures are not well developed, and trends may vary as much as forty-five degrees. The overall orientation is in a plane

perpendicular (fig. 13) to the large northwestward trending fault. For this reason they are classified as BC joints.

The exact attitude of the fault (map 2) is unknown. It strikes to the northwest, and the dip appears to be near vertical. Weathering along the fault plane prohibited a better estimate of the dip.

The secondary quartz axes (fig. 15, 22, and 26) are weakly confined to a plane perpendicular to the attitude of the joints. The weak fabric pattern may be due to a final adjustment in the area after the faulting.

STATISTICAL ANALYSIS

Most of the statistical analyses applied to petrofabric work have been directed toward resolution of the individual fabric pattern, to determine whether the fabric is isotropic or anisotropic. This analysis is useful only in cases where the nature of the pattern is not clear. The results obtained from samples collected from the outcrop below the dam show a very strong preferred orientation of the microfractures. Therefore, it was not necessary to approach the problem with this type of analysis. Descriptions of the methods used for analysis of weak patterns are given by Fairbairn (1954), Chayes (1946), and Krumbein (1939).

Use of a Chi-square test for comparison of diagrams is limited. Most authors suggest that each cell must contain at least five values before a Chi-square test may be applied. In petrofabric work, a cell which contains zero points may be as significant as a cell which contains several points. However, limited comparisons may be made between similar cells if each contains five or more points, but the results may not reflect the true relationship between the diagrams. This is especially true in cases where comparison is made between two diagrams that show a very strong preferred orientation.

In this study, a comparison is made between the orientation of the fractures on the fold and those adjacent to the fault. Since it is believed that the major system of fractures is associated with the secondary folding, there should be no significant difference in their orientation. The fractures on the fold (fig. 12) trend northeastward; while adjacent to the fault (fig. 13) the maxima indicate a trend of a few degrees east of north. Comparison was made by assuming that the fractures are older than the drag folds, and therefore, the beds from which the samples were collected had the same attitude at the time of fracturing. It is convenient, in this case, to rotate the beds to an east-west vertical position for analysis.

The analysis was carried out in the following manner.

1. The fracture diagrams were placed into two main groups.
    a. Location 1 - fractures in the fold limbs. (fig. 2-5)
    b. Location 2 - fractures adjacent to the fault. (fig. 6-8)
2. All of the diagrams were rotated so the bedding had an east-west vertical attitude.
3. Two composite diagrams were made from the rotated diagrams.
4. The two composite diagrams were then compared by determining the rank correlation coefficient. Three separate tests were made using different grid systems.

The type of grid used is not important. The main factor is the numbering of the individual cells; for the number

of points found in each cell is the basis for comparison. However, the area each cell encloses will directly effect the accuracy of the test. For example, a test in which each cell of the grid contains five percent of the area will not reveal a coefficient of correlation as valid as one obtained by using a grid in which each cell contains one percent of the total area. This test does not determine the nature of the fabric pattern. It is used only as a basis for comparison. For example, in testing two diagrams which possess random orientation, the coefficient of correlation is likely to be significant. This merely points out a similarity which exists between the two fabrics.

The three grids (fig. 34) used in the rank correlation tests were constructed so that each cell contained one percent, two percent, and five percent respectively of the total area of the diagram. Since the ten centimeter Schmidt net

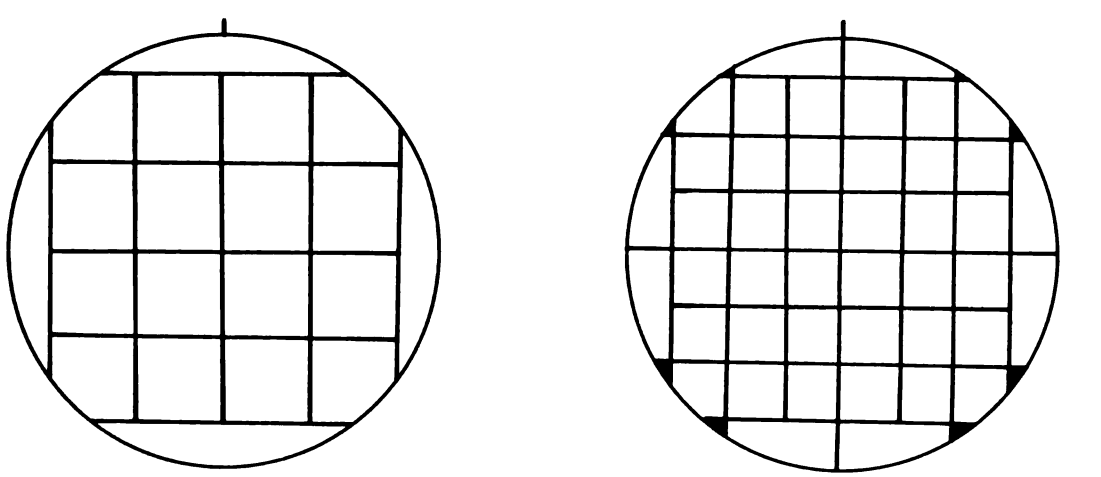

Fig. 34 Five and two percent grids used for counting points in the statistical analyses.

was used for plotting the points, the sides of each cell were 1.77 centimeters, 2.51 centimeters, and 3.69 centimeters long respectively. The cells were numbered, and the number of points lying within each cell was recorded in a table similar to Table V. The sum of the squares of the difference of ranks could then be computed and the results placed in the equation:

$$R = 1 - \frac{6(\Sigma D^2)}{N(N^2-1)}$$

where R is the rank coefficient of correlation, D is the difference between ranks, and N is the number of pairs.

TABLE V

DETERMINATION OF ΣD^2 USING

THE FIVE PERCENT GRID

Cell number	X f from Loc #1	Y f from Loc #2	Rank of X	Rank of Y	D R_x-R_y	D^2
1	3	0	7.5	3.5	4.0	16.00
2	2	0	3.0	3.5	0.5	0.25
3	3	0	7.5	3.5	4.0	16.00
4	3	1	7.5	7.5	0.0	0.00
5	0	0	1.0	3.5	2.5	6.25
19	8	2	14.0	9.0	5.0	25.00
20	7	1	13.0	7.5	5.5	30.25
					ΣD^2	= 304.00

Results obtained from this test appear in Table VI.

The following formula, from Baten (1938), was used for testing the significance of the coefficient of correlation:

$$\sigma_R = \frac{1-R^2}{N}(1 + .086R^2 + .013R^4 + .002R^6)$$

where R is the rank coefficient of correlation, N is the number of pairs, and σ_R is the standard error of estimate. In order that the coefficient of correlation be significantly different from zero, R must be two to three times greater than the standard error of estimate.

TABLE VI

COMPARISON OF RANK COEFFICIENT OF CORRELATION WITH STANDARD ERROR OF ESTIMATE

% area	Rank Coeff. of Correlation (R)	Standard error of estimate (σ_R)	R/σ_R
1	.5522	.074	7.45
2	.5817	.103	5.63
5	.7715	.137	5.60

The results in Table VI indicate a positive correlation between the two fabric diagrams at all percentage levels. On the basis of this test, it may be assumed that the major set of fractures on the fold limbs, and the fractures adjacent to the fault are from the same population.

SUMMARY

There are at least three ages of fractures in the iron-formation which is exposed immediately below the Crystal Falls municipal dam. The oldest, and most prominent, are believed to be AC tension joints related to the nearly east-west secondary folding. If this is the case, the fracture pattern is the result of a north-south horizontal compression accompanied by an east-west stretching along the fold axis. Since formation, some of the fractures (sample numbers 1, 2, 3, and 4) in this group have been rotated by subsequent drag folding. The fractures in the area adjacent to the northwestward trending fault have not been affected by drag folding, and are believed to represent the orginal orientation of the joints in this classification.

The fractures of intermediate age are not extensive, and therefore are not well defined in the fabric diagrams. This age of fracturing includes two types of joints which are believed to be contemporaneous. One type is found only in the apical region of the drag fold, and are thought to be AB tension joints. The second type of fracture is parallel to the bedding, and is the result of parting or splitting between individual beds. The intersection of these joints produce a lineation in the B direction of the drag fold.

The third, and youngest, set is found in a plane generally perpendicular to the attitude of the large northwestward trending fault which cuts across the outcrop. These fractures are probably BC joints associated with the faulting. They have a northeast trend, and dip gently to the northwest.

The sequence of tectonic activity in the area based on the results of this study would be as follows.

Paratectogensis of the
Crystal Falls Area

Regional subsidence		----------
Regional faulting		-------
Secondary folding	(AC joints)	-----
Drag folding	(AB joints)	-----
Faulting	(BC joints)	-----

The close of the Huronian period is marked by a regional subsidence accompanied by large scale faulting. The next tectonic activity resulted in the formation of a series of nearly horizontal east-west folds in the northern Crystal Falls area. At this time, a prominent set of north-south vertical fractures developed. These fractures were filled with secondary quartz before drag folding. The compressional forces during this period were from the north and south. A stretching along the axes of the folds produced the AC tension joints.

During the period of drag folding, a second set of joints was developed. Actually, two types of joints are included in this period. One type is subparallel to the axial plane of the drag fold, and the other is parallel to the bedding. Both types are tension features. The drag folding is the result of an east-west couple.

The drag folding was closely followed by faulting. The faulting is subparallel to the axial plane of the drag fold, and may be a result of shear at a time when the iron-formation was competent. The third set of fractures, believed to be BC joints, are related to this period of faulting.

PLATE I

A. Displacement has occurred along the fractures, followed by quartz mineralization. The horse-tail fault and displacement of the northwest trending quartz filled fracture indicate the apparent direction of movement. The larger fracture contains quartz growing perpendicular to the fracture walls. Oxidation has taken place along bedding, and some of the fractures. Plain light, X3. Sample #2, slide B.

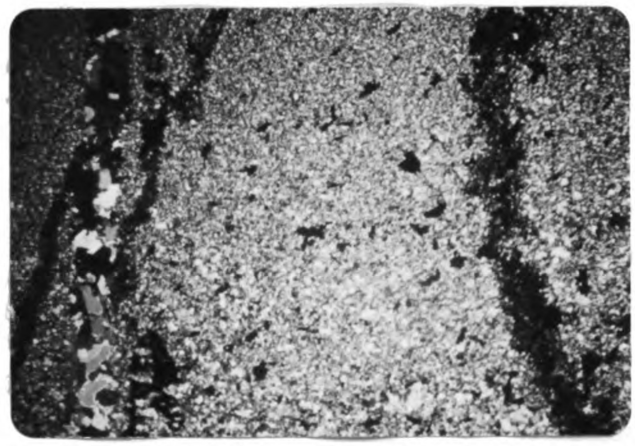

B. A hematite filled fracture displaced by a fracture containing quartz. The fine chert mosaic with inclusions of hematite is typical of the unoxidized iron-formation. Crossed nicols, X2. Sample #2, slide B.

PLATE II

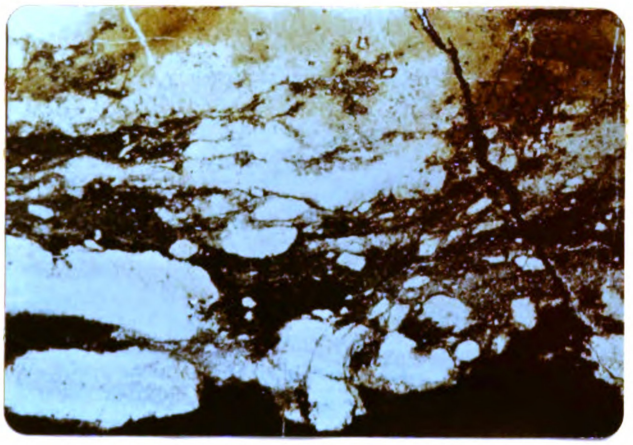

A. Pseudo-stretched-pebbles (?) believed to have formed as a result of slippage parallel to the bedding. The surrounding matrix is composed of chert, siderite, hematite, and iron silicates. The large veinlet contains hematite. Plain light, X2. Sample #5, Slide A.

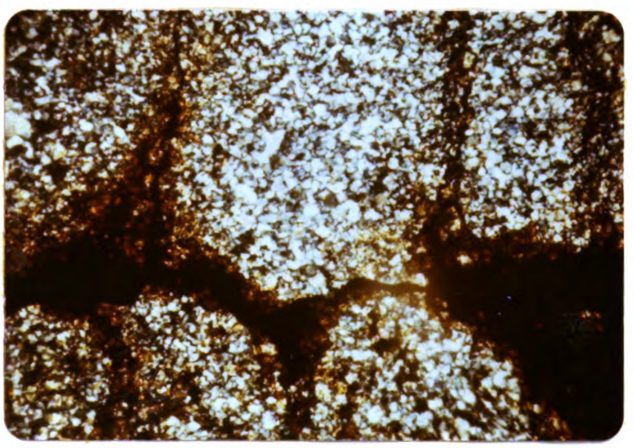

B. Internal structure of the pseudo-stretched-pebbles. Hematite (black) has formed along fractures within the pebble. Crossed nicols, X2. Sample #5, slide A.

PLATE III

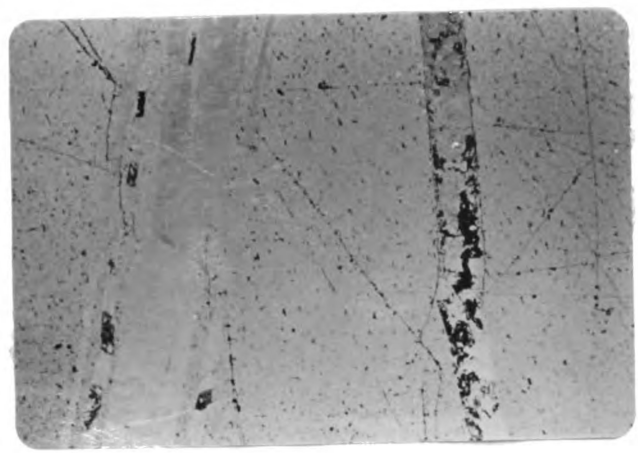

A. Fractures containing secondary quartz transecting several smaller fractures. The large fracture to the right developed along a pre-existing fracture. Black minerals in the large fracture are hematite and pyrite. Hematite in the cherty matrix has a slight elongation from northwest to southeast. Plain light, X3. Sample #2, slide C.

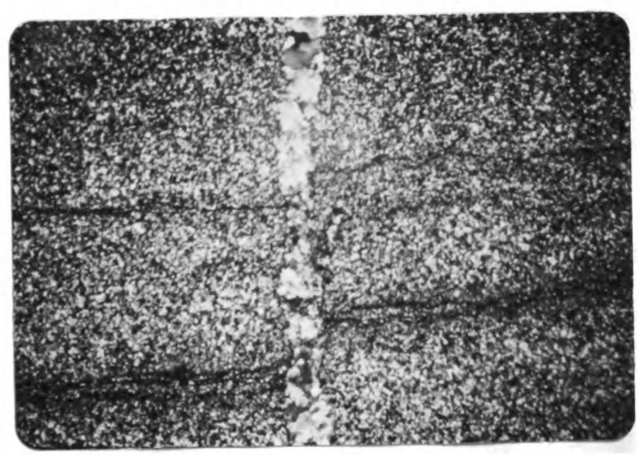

B. Displacement of bedding by movement along a fracture. Crossed nicols, X2. Sample #7, slide A.

PLATE IV

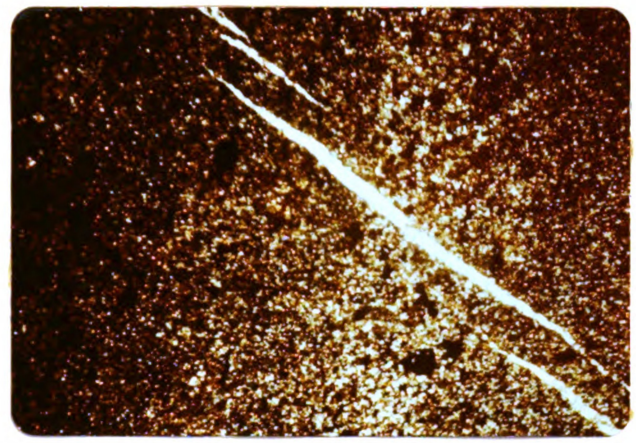

A. En echelon fracture in mylonitized iron-formation. This type of fracturing is common in the apical region of the drag fold. The mylonitic character of the iron-formation is present only at the apex of the fold (sample #3), and in the area immediately adjacent to the fault (sample #5). Without analyzer, X2. Sample #3, slide A_1.

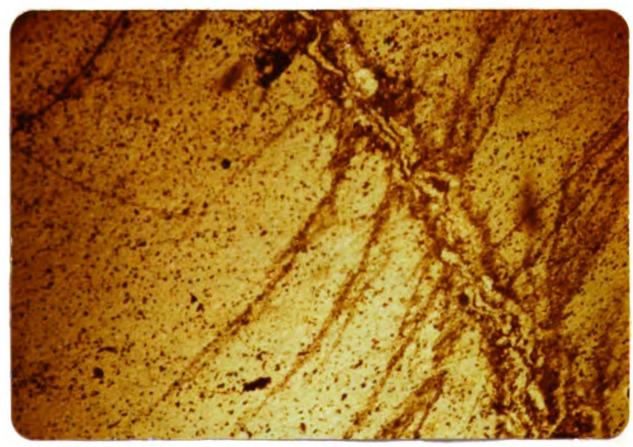

B. Feather joints (Hills, 1953). The main fracture is probably due to shear, and the branching resulted from accompanying tension. These fractures are called pinnate shear, and pinnate tension joints respectively. The acute angle between the shear direction and the tension fracture points in the direction in which the block moved. Without analyzer, X2. Sample #7, slide C.

PLATE V

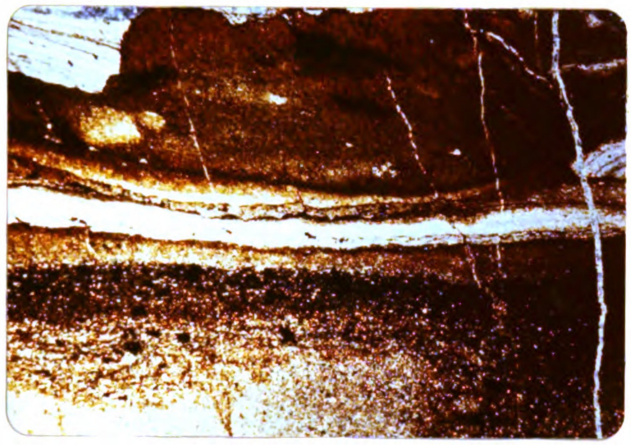

A. Structures associated with rock flowage. All of the fractures are younger than the features due to the period of flowage. Plain light, X3. Sample #6, slide A.

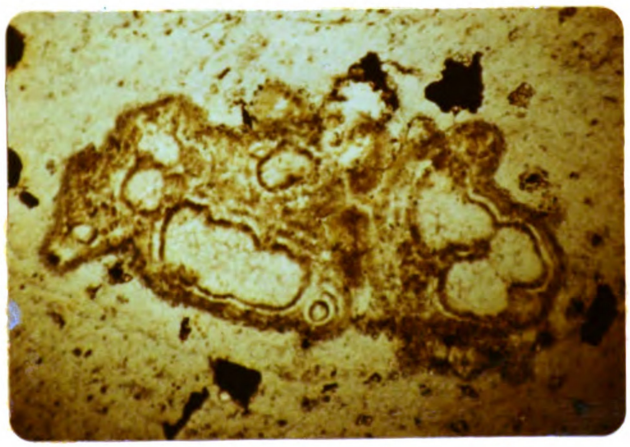

B. Algal structure (?). This feature is limited to a very narrow horizon, and was observed only in one sample. Without analyzer, X12. Sample #2, slide B.

PLATE VI

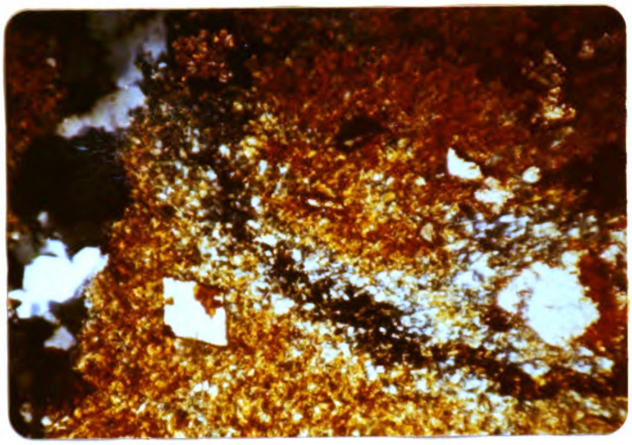

A. Siderite rhombohedron in chert with limonite stain. The siderite is being altered to limonite through normal weathering processes. Oxidation of the iron silicates to limonite is responsible for much of the coloring in this section. Crossed nicols, X2. Sample #2, slide B.

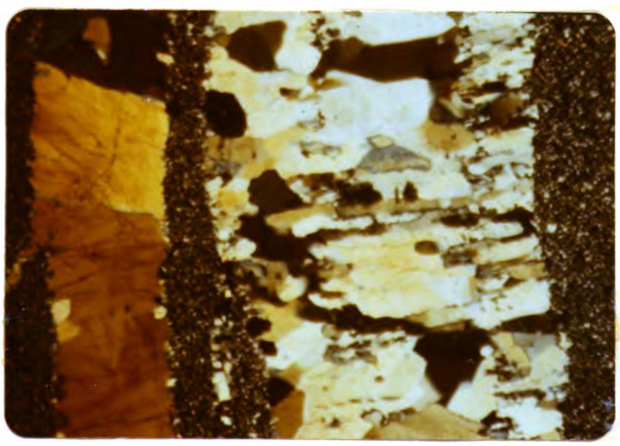

B. Quartz growing perpendicular to the fracture walls. The quartz occurs in two distinct grain sizes, but there is no difference of orientation of the c-axes. Crossed nicols, X2. Sample #2, slide B.

PLATE VII

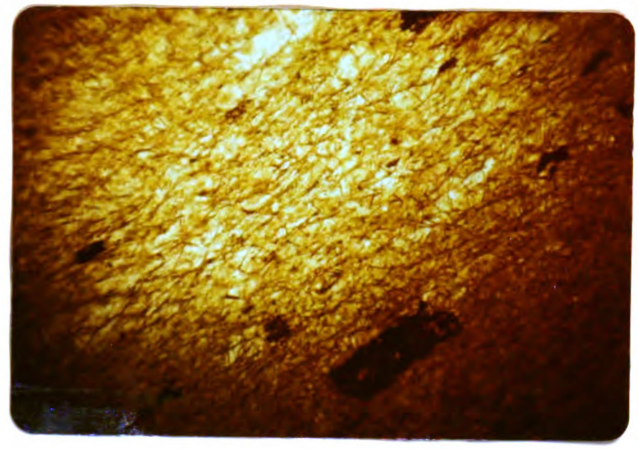

A. Needles of stilpnomelane and minnesotaite disseminated in chert. The black to rust colored mineral is hematite. Without analyzer, X12. Sample #4, slide C.

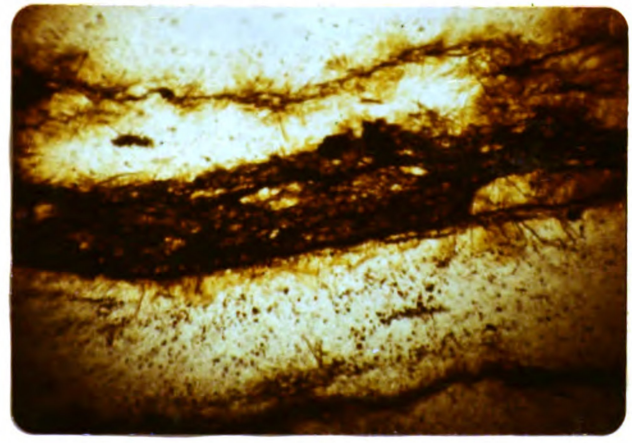

B. Yellowish-green stilpnomelane in radiating needles. The brown-black mineral is primary hematite which occurs in many of the bedding planes. In limited cases, the needle-like mineral displayed no pleochroism, and for this reason is tentatively called minnesotaite. Without analyzer, X12. Sample #4, slide B.

BIBLIOGRAPHY

Balk, Robert. (1952) Fabric of Quartzites near Thrust Faults; Journal of Geology, Vol. 60, p. 415.

Baten, W.D. (1938) Elementary Mathematical Statistics; Wiley and Sons, Inc., New York.

Billings, M.P. (1954) Structural Geology; Prentice-Hall, Inc., New York.

Chayes, Felix. (1946) Application of the Coefficient of Correlation to Fabric Diagrams; Transactions of the American Geophysical Union, Vol. 27, p. 400.

Dutton, C.E. (1950) Progress of Geologic Work in Iron and Dickinson Counties, Michigan; U.S.G.S. Circ. 84.

Fairbairn, H.W. (1954) Structural Petrology of Deformed Rocks; Addison-Wesley Publishing Co., Cambridge, Mass.

Gruner, J.W. (1946) The Mineralogy and Geology of the Taconites and Iron Ores of the Mesabi Range, Minnesota; Office of the Commissioner of the Iron Range Resources and Rehabilitation, St. Paul, Minn.

Hills, E.S. (1953) Outlines of Structural Geology; Methuen and Co., Ltd., London.

Krumbein, W.C. (1939) Preferred Orientation of Pebbles in Sedimentary Deposits; Journal of Geology, Vol. 47, p. 673.

Pettijohn, F.J. (1946) Geology of the Crystal Falls - Alpha Iron-bearing District, Iron County, Michigan; U.S.G.S. Strategic Mineral Investigation Preliminary Map 3-181.

Pettijohn, F.J. (1952) Geology of the Northern Crystal Falls Area, Iron County, Michigan; U.S.G.S. Circ. 153.

Tuttle, O.F. (1950) Preparation of Oriented Thin Sections; Journal of Geology, Vol. 58, p. 73.

Tuttle, O.F. (1955) Professor, Pennsylvania State University, written communication.

Williams, H., Turner, F.J., and Gilbert, C.M. (1954) Petrography; W.H. Freeman and Co., San Francisco.

Winchell, A.N., and Winchell, H. (1951) Part II, Elements of Optical Mineralogy; Wiley and Sons, Inc., New York.

Zinn, Justin. (1932) Correlation of the Upper Huronian of the Marquette and Crystal Falls Districts; Michigan Academy of Science, Arts, and Letters, Vol. 18, p. 437.